Characterizing the ratio of nitrate to sulfate in ambient fine particles of urban Beijing during 2018–2019

Shangze Li [a], Fang Zhang [a,*], Xiaoai Jin [a], Yele Sun [b,c], Hao Wu [a], Conghui Xie [b,c], Lu Chen [a], Jieyao Liu [a], Tong Wu [a], Sihui Jiang [a], Maureen Cribb [d], Zhanqing Li [d]

[a] College of Global Change and Earth System Science, Beijing Normal University, Beijing, 100875, China
[b] State Key Laboratory of Atmospheric Boundary Layer Physics and Atmospheric Chemistry, Institute of Atmospheric Physics, Chinese Academy of Sciences, Beijing, 100029, China
[c] University of Chinese Academy of Sciences, Beijing, 100049, China
[d] Earth System Science Interdisciplinary Center and Department of Atmospheric and Oceanic Science, University of Maryland, College Park, MD, USA

HIGHLIGHTS

- The ratio of NO_3^- to SO_4^{2-} in 2018–2019 declined.
- A continuous increase in the ratio of NO_3^- to SO_4^{2-} of 1999–2018 is presented.
- The reduction measures in place serve only to improve SO_4^{2-} pollution in winter.
- High SO_4^{2-} levels are still observed in summer.

ARTICLE INFO

ABSTRACT

A variety of legislative actions for air quality improvement have been conducted in China since 2013, and the emission control measures have achieved remarkable reduction in severe haze frequency. The composition of the fine particles may change along with the improved air quality, and thus may induce distinct environmental and climate effects in future. In this study, a very recent long-term dataset (2018–2019) of non-refractory chemical composition measured by a quadrupole aerosol chemical speciation monitor (Q-ACSM) observed in urban Beijing is applied to investigate the changes in ratio of nitrate (NO_3^-) to sulfate (SO_4^{2-}) in $PM_{2.5}$ (particulate matter with diameters of less than 2.5 μm). We show that the ratio of NO_3^- to SO_4^{2-} varies seasonally, with a maximum in winter (1.6 ± 1.2) and a minimum in summer (0.7 ± 1.0). Compared with results from earlier studies showing a continuous increase in the ratio of NO_3^- to SO_4^{2-} since 1999, a decline in the ratio is found during the period of 2018–2019. This is partially associated with an attenuated nitrate formation likely due to reduced nitrogen oxides emissions since 2016 in China. Our results suggest that the strict reduction control measures in place serve only to improve SO_4^{2-} pollution in winter but not in summer when high SO_4^{2-} levels are still observed. SO_4^{2-} and NO_3^- concentrations during study periods together comprise 37–53% of $PM_{2.5}$, presenting significant role in dominating the levels of $PM_{2.5}$. In addition, we show that the ratio of NO_3^-/SO_4^{2-} in warm seasons generally increases with increasing relative humidity (RH) due to enhanced NO_3^- hydrolysis formation, but with a maximum value of only ~1.0 that is pulled down by the high levels of sulfate in summer, while the dependence of the ratios on RH is more pronounced in cold seasons when multiple factors (regional transportation, planetary boundary layer, PBL and sources of sulfate, etc.) can impact nitrate levels. We finally characterize two typical processes that lead to the rapid accumulation of nitrate in the atmosphere over urban Beijing: the regional transportation and PBL variations, which is found driving heavy haze in cold seasons, and the hydrolysis formation and partitioning of NO_3^- that tends to impact the diurnal patterns of nitrate in warm seasons.

1. Introduction

Haze pollution, which is characterized by high-levels of chemical components in fine aerosols, has occurred frequently in China (Yang et al., 2011; Sun et al., 2012; Guo et al., 2014; Wang et al., 2019a; Zhang et al., 2020) and profoundly impacts human health, weather, and climate (IPCC, 2013; WHO, 2018). Air quality is inherently regulated by the synergetic effects of emissions, chemistry, transport, and removal of pollutants (Zhang et al., 2018, 2020).A variety of legislative actions for air quality improvement have been conducted in China since 2013, and the emission control measures have achieved remarkable reduction in severe haze frequency (Zhang et al., 2019), but analysis of long-term measurements in China indicates no improving trend for moderate haze events (Zhang et al., 2020).

The composition of the fine particles may change along with the improved air quality, and thus may induce distinct environmental and climate effects in future. For example, the proportion of nitrate (NO_3^-) in $PM_{2.5}$ has been observed steadily increasing (Xu et al., 2019a; Wang et al., 2017) because the emission reduction measures in China are mainly aimed at sulfur dioxide (SO_2), suggesting different changes in the ratios of each individual chemical component in PM under the scenario of emission reductions in China. Compared with SO_2, the emission of high concentrations of nitrogen oxides (NO_x) and gaseous ammonia (NH_3) has not attracted much attention from the Chinese government (Itahashi et al., 2018), likely resulting in the increasing proportion of NO_3^- in secondary inorganic aerosols (SIA). For example, P. Xu et al. (2018) observed multiple NO_3^- pollution processes (~60 µg m^{-3} out of the total concentration of NR-PM$_1$) in the autumn of 2017. Xu et al. (2019a, b) showed that the proportion of NO_3^- in NR-PM$_1$ increased continuously from 2011 to 2019 based on long-term ACSM observations. This suggests that with strong emission reduction measures in place in Beijing, the formation of haze with sulfate (SO_4^{2-}) as the main pollutant has transitioned to a pollution process with NO_3^- as the main pollutant (Li et al., 2019; Xu et al., 2019a). However, recently, a few isolated cases have been reported where the proportion of SO_4^{2-} in Beijing's pollution is still higher than that of NO_3^- (Wang et al., 2019b; Xu et al., 2018). A most recent study reveals that efficient sulfate formation from black carbon catalyzed SO_2 oxidation in the presence of NO_2 and NH_3, even at very low SO_2 levels (down to a few ppb) and an intermediate RH range (30–70%) (Zhang et al., 2020), implying that reduction of SO_2 alone is insufficient in mitigating sulfate formation and haze occurrence. In the context of strong emission reduction, understanding the variations in chemical characteristics of fine aerosols is crucial to understand the chemical/physical processes leading to haze formation, and to help devising more effective mitigation strategies.

The sulfate and nitrate are two major SIA of $PM_{2.5}$ in the atmosphere (An et al., 2019). Current research indicates that NO_3^- in the ambient atmosphere is formed through three pathways, i.e., the photochemical oxidation of nitrogen dioxide (NO_2) by OH radicals in the daytime (Morgan et al., 2015), and the heterogeneous formation through the nitrous oxide (N_2O_5) hydrolysis reaction at night (Wang et al., 2018; Yun et al., 2018), and on the surfaces of dust aerosols (Xia et al., 2019; Tang et al., 2012).

The sources and formation mechanism of NO_3^- is relatively clearer than that of SO_4^{2-}. The dispute about NO_3^- mainly focuses on the contribution of two pathways, the heterogeneous hydrolysis of N_2O_5 at night and photochemical oxidation during the day, to the ambient levels of NO_3^- in urban areas. For the sulfate, it is formed from both the gas-phase oxidation of SO_2 by OH radical that is with a period of about 1 week, and from heterogeneous reactions in the aqueous phase of clouds, fog, and aerosols (Zhang et al., 2015a). In addition, it also shows that residential coal burning has been an important source of primary sulfate in the atmosphere in winter of north China (Dai et al., 2019). Meteorological conditions (winds, RH) and variations in the height of the planetary boundary layer (PBL) will also cause rapid increases in NO_3^- and SO_4^{2-} mass concentrations in a short period (Zhang et al., 2019;
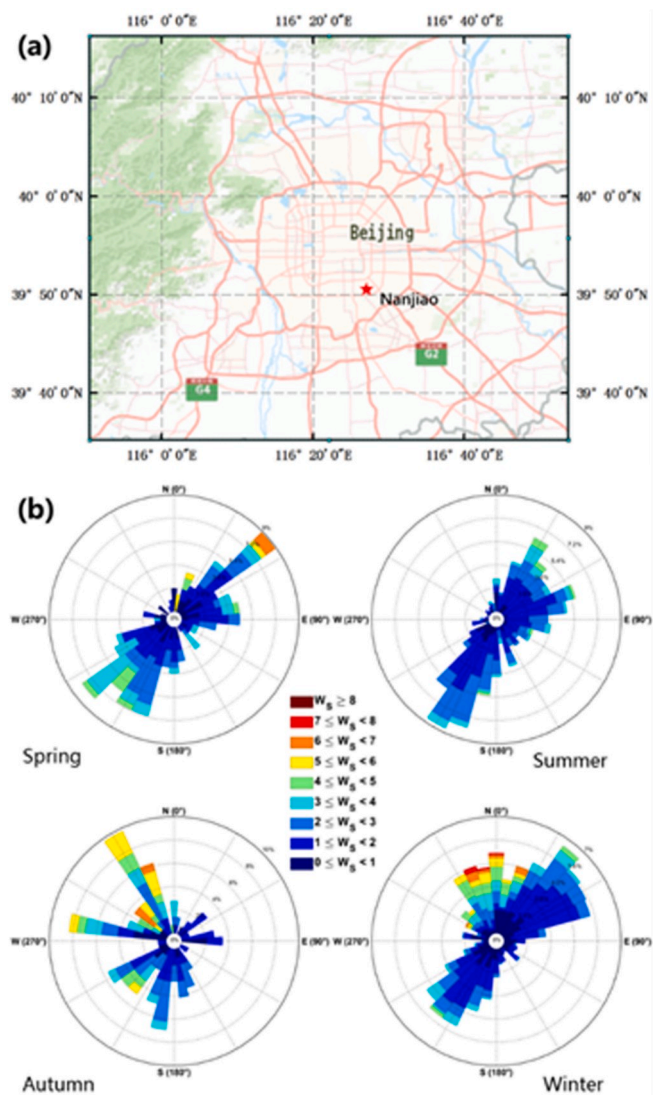

Fig. 1. (a) Map of the area surrounding the sampling site (Nanjiao), made by ArcGIS (https://www.arcgis.com/index.html#). **(b)** Wind rose plots for each season. The color bar is wind speed (w$_s$, m s^{-1}). (For interpretation of the references to color in this figure legend, the reader is referred to the Web version of this article.)

Zhong et al., 2018; Wang et al., 2015; Zhang et al., 2020). Since NO_3^- is volatile, changes in temperature will also affect its formation process and concentration. Based on wintertime observations, Guo et al. (2016) found that temperature changes had no significant impact on the gas-particle partitioning of NO_3^-, so the concentration of NO_3^- was not affected. However, Y. L. Sun et al., 2013a concluded that the NO_3^- concentration was correlated to RH and inversely correlated with temperature based on long-term observations. More importantly, the formation of SO_4^{2-} can affect the formation of NO_3^- by changing the gas-particle partitioning (Vasilakos et al., 2018; Li et al., 2018). With the decline of ambient SO_4^{2-} levels, NO_3^- formation may be inhibited. Therefore, it is important to explore how these multiple factors affect the partitioning of NO_3^- in different seasons or in different periods under the scenario of strict reduction measures in China. This will help better simulate the two major inorganic salts in models.

In this study, we used a quadrupole-ACSM (Q-ACSM) to measure NR-$PM_{2.5}$ with a 2.5 µm lens in the urban area of Beijing from March 2018 to February 2019. The temporal variations (seasonal and diurnal) in the mass concentrations of NO_3^- and SO_4^{2-} in submicron aerosols were
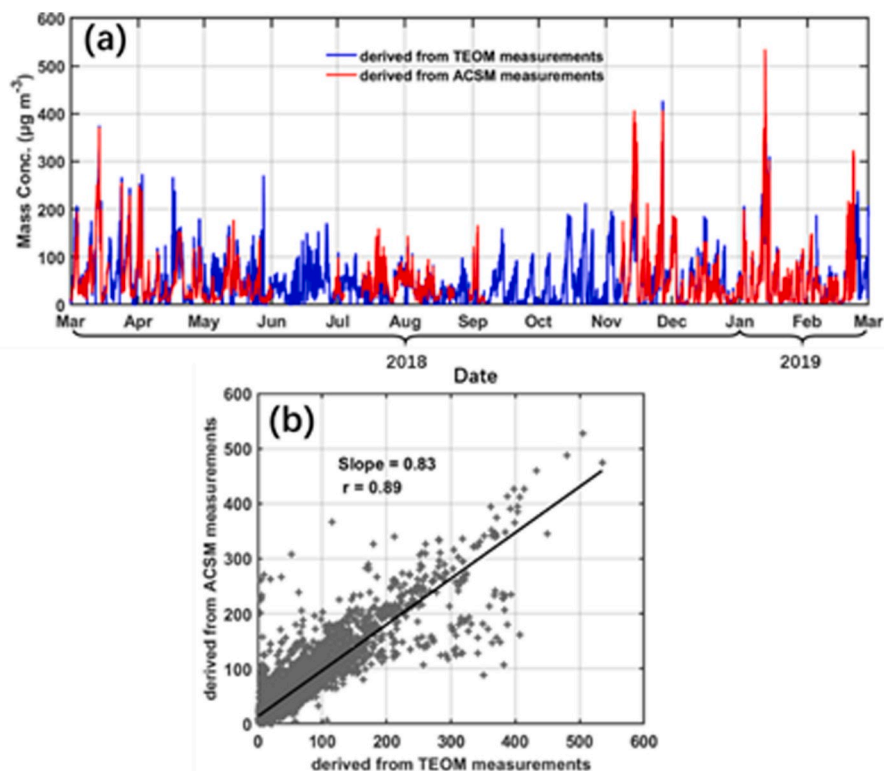
Fig. 2. (a) Time series of NR-PM$_{2.5}$ and PM2.5 concentrations concentration measured at the Nanjiao sampling site derived from Q-ASCM (in red) and TEOM technique (in blue). The measurements of PM$_{2.5}$ concentration by TEOM is conducted at a site nearby the Nanjiao sampling site; (b) Correlation of NR-PM$_{2.5}$ and PM$_{2.5}$ concentrations obtained by the two instruments. The black line is the best-fit line from linear regression. The slope of the line and the correlation coefficient (r) are shown. (For interpretation of the references to color in this figure legend, the reader is referred to the Web version of this article.)

characterized, with a focus on the changes in the ratio of NO_3^- to SO_4^{2-} to investigate the effect of emission control measures on these two major SIAs in urban Beijing. The dependence of the ratio of NO_3^- to SO_4^{2-} on temperature (T) and RH in cold and warm seasons was also examined to obtain insights into the effect of these factors on NO_3^- and SO_4^{2-} levels. Finally, a case study was conducted to elucidate the effects of regional transport, the PBL, and chemical processes on the rapid growth of SIAs in urban Beijing.

2. Site and measurements

2.1. Sampling site and instruments

We conducted long-term measurements from 1 March 2018 to 23 February 2019 on the campus of the Atmospheric Exploration of the China Meteorological Administration (39°48′34″N, 116°28′49″E) (Fig. 1a). The sampling site was located between the southern fourth and fifth ring roads, which is frequently influenced by vehicle emissions. Air masses transported from Hebei Province, south of Beijing, which are heavily polluted because of the emissions from industries and anthropogenic sources, pass over the site. Wind roses (Fig. 1b) show that horizontal winds at the site are dominantly from the northeast and southwest in spring, summer, and winter (Fig. 1b). Winds from the north can also occur in winter. In autumn, the dominant winds are from the northwest and south. A large number of instruments were installed in a container deployed at the site for measuring aerosol physical and chemical properties, including a Q-ACSM, scanning mobility particle sizers, an aerodynamic particle sizer (model 3321, TSI), a hygroscopic and volatile tandem differential mobility analyzer (H/V-TDMA), a cloud condensation nuclei counter (CCNc-100), an eddy covariance flux meter (model 7500A, LI-COR Environmental), and a Raman Lidar.

The eddy covariance flux meter measured meteorological parameters, including wind speed (WS), wind direction (WD), T, and RH. The highest T during the observation period was close to 40 °C (in summer), and the lowest T was close to −10 °C (in winter). RH was high in summer, with an average value of 69%, and low in winter, with an

average value of 38%. Black carbon (BC) was measured by an aethalometer (model AE-33, Magee Scientific) at the Institute of Atmospheric Physics, Chinese Academy of Sciences. Ammonia (NH_3) data were collected using an NH_3 analyzer (model EC9842, Ecotech) installed at the campus of the China Meteorological Administration.

Atmospheric particle concentrations, including PM$_{2.5}$ and PM$_{10}$, and collocated gaseous species, including CO, ozone (O_3), NO_2, and SO_2, were measured simultaneously at the Yizhaung provincial control station (Yizhuang site) by various gas analyzers from the Ministry of Ecology and Environment (MEE, http://www.mee.gov.cn/hjzl/), with a temporal resolution of 1 h. The Yizhuang site is very close to our observation site (3.5 km). All observation data were further processed and analyzed at 24-h intervals according to the PM$_{2.5}$ sampling time.

2.2. ACSM data calibration and analysis

In this study, real-time NR-PM$_{2.5}$, including organics (Org), nitrate (NO_3^-), sulfate (SO_4^{2-}), ammonium (NH_4^+), and chloride (Chl), were first measured in Beijing with a PM$_{2.5}$-Q-ACSM equipped with a capture vaporizer (CV). Compared with the standard vaporizer (SV), the CV can effectively reduce the bounce times of particles, thus reducing the loss of detected particles (Hu et al., 2017, 2018). Zhang et al. (2017) have demonstrated the usefulness of data measured by a PM$_{2.5}$-Q-ACSM equipped with a CV. An ammonium sulfate solution was used for the calibration of the ACSM to determine its response factor and relative ionization efficiency (RIE). After passing through the aerodynamic lens, the CV vaporized all particles (Ng et al., 2011).

The average lowest detection limits of the ACSM in 30 min are 0.54, 0.06, 0.07, 0.25, and 0.03 μg m^{-3} for Org, NO_3^-, SO_4^{2-}, NH_4^+, and Chl (Sun et al., 2012). All of the NR-PM$_{2.5}$ species were preprocessed using the Igor Pro-ACSM. Default RIEs of 1.4 for Org, 1.1 for NO_3^-, and 1.3 for Chl (Allan et al., 2003; Drewnick et al., 2005). Our calibration determined an RIE of 5.57 for NH_4^+ and an RIE of 1 for SO_4^{2-}, which were used rather than default values so that more accurate data on SO_4^{2-} and NH_4^+ could be obtained. The collection efficiency (CE) is set to 0.5, a value applicable to field observations (Drewnick et al., 2005; Jayne et al.,
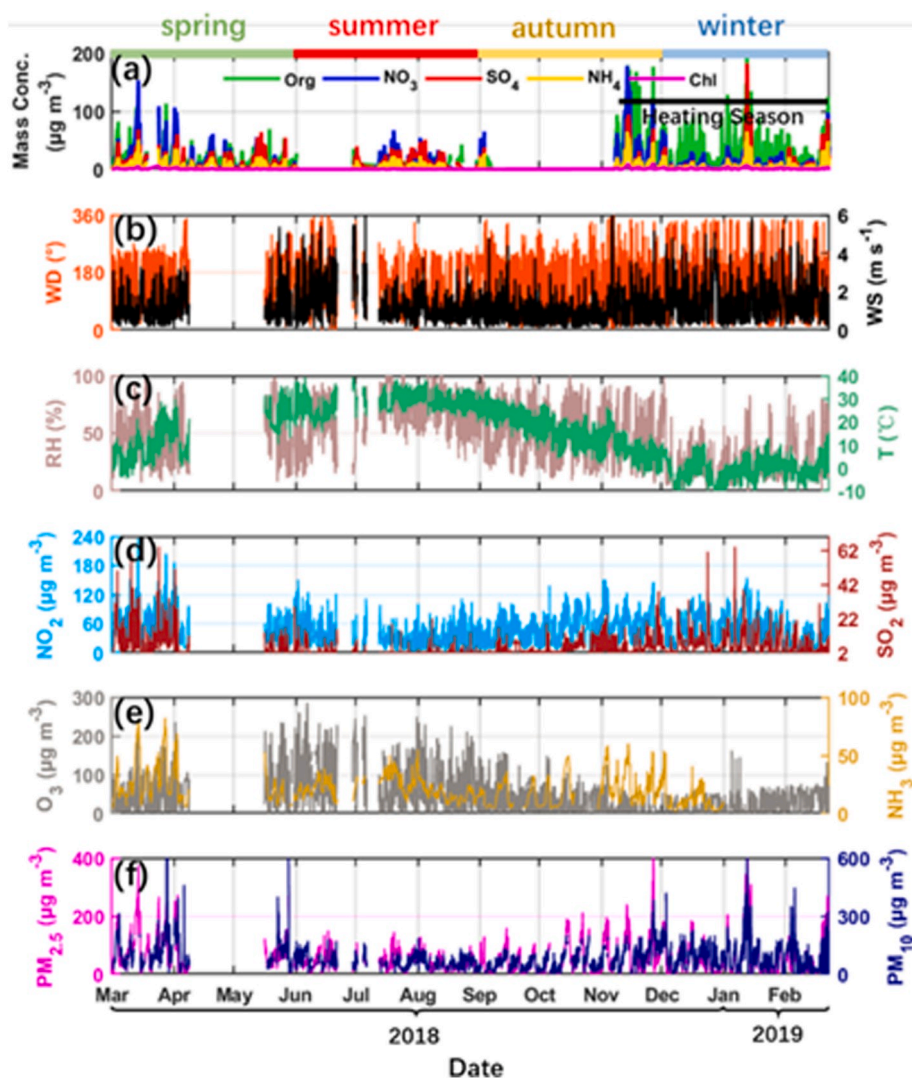
Fig. 3. Time series of **(a)** NR-PM$_{2.5}$ species at the ground level, **(b)** wind direction (WD) and wind speed (WS), **(c)** relative humidity (RH) and temperature (T), **(d)** NO$_2$ and SO$_2$, **(e)** O$_3$ and NH$_3$, and **(f)** PM$_{2.5}$ and PM$_{10}$ in Beijing from 2018 to 2019.

2000; Xu et al., 2015; Sun et al., 2015a). Because the CV is an improvement over the SV, the CE can be improved for ambient particles in the ACSM. A recent evaluation of CV values measured by inorganic species showed consistent results with measurements made in the same area (Hu et al., 2017). Therefore, in this study, we used the CE of the SV, i.e., CE = 1 (Xu et al., 2016; Hu et al., 2017). To reduce the uncertainty of the CE, we added a Nafion dryer under the aerosol inlet, reducing the sampling humidity of aerosols to less than 40% (Sun et al., 2015a, 2015b).

Fig. 2 shows the time series of and comparisons between NR-PM$_{2.5}$ concentrations measured at the Nanjiao sampling site and PM$_{2.5}$ concentrations measured at the nearby Yizhuang site. The annual trends (Fig. 2a) and concentrations (Fig. 2b) at the two sites match well (slope of the linear regression fitting is 0.83, and the correlation coefficient is 0.89). Due to the lack of BC data during the observation period, the concentration of NR-PM$_{2.5}$ observed by the ACSM at Nanjiao is slightly less than that of PM$_{2.5}$ measured at Yizhuang site. Note that in the autumn of 2018, the ACSM aerosol inlet was blocked, and only a small amount of data was obtained at that time.

3. Results and discussion

3.1. Measured time series of chemical components and meteorological parameters

Fig. 3 shows the time series of mass concentrations of chemical components, meteorological conditions, and concentrations of trace gases and particulate matter (PM$_{2.5}$ and PM$_{10}$) from 2018 to 2019. All of the chemical components measured varied throughout the year, showing large fluctuations with changing meteorological conditions and trace gas concentrations. This results in large variations in the mass concentrations of PM$_{2.5}$ and PM$_{10}$. Overall, more and higher spikes of mass concentration of the chemical components were observed in winter and spring. Because of the malfunction, only few data is obtained in autumn and it may not well represent the circumstances in this season.

3.2. Seasonal variation

Fig. 4 shows the seasonal variations in mean mass concentrations of NO$_3^-$ and SO$_4^{2-}$, the ratio of NO$_3^-$ to SO$_4^{2-}$, and the mass fractions of the chemical components. No obvious seasonal variations are observed in both the average mass concentration and the fraction of NO$_3^-$, with ranges of ~10–12 μg m^{-3} and 22–26%, respectively. A slightly greater
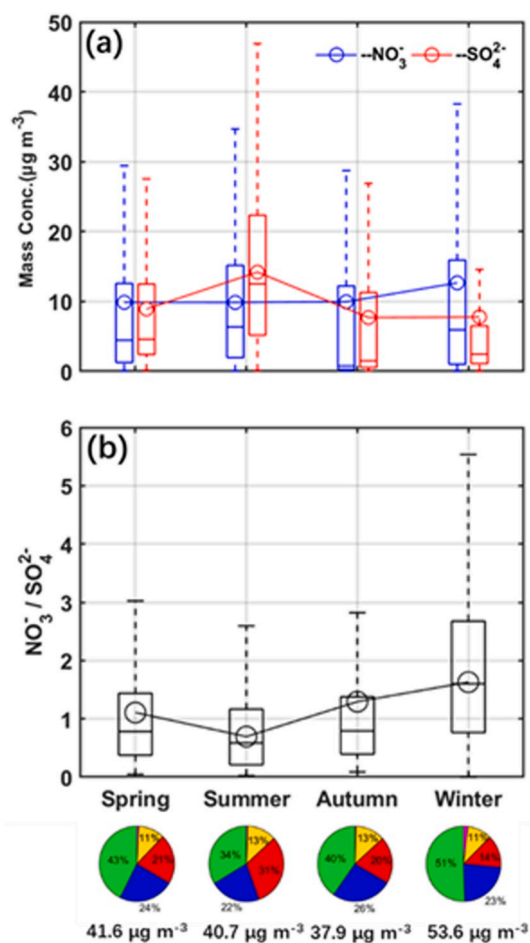
Fig. 4. Seasonal variations in **(a)** NO_3^- (blue) and SO_4^{2-} (red) mass concentrations and **(b)** the ratio NO_3^-/SO_4^{2-}. Horizontal lines in the box plot represent the median values, the circles represent the mean values, upper and lower borders of the box represent the 25th and 75th percentile values, and the upper and lower borders of the dashed vertical lines represent the 10th and 90th percentile values. The pie charts at the bottom show the average mass fractions of the chemical composition of NR-PM$_{2.5}$ in each season. The mean mass concentration of NR-PM$_{2.5}$ for each season is also shown below the pie charts. (For interpretation of the references to color in this figure legend, the reader is referred to the Web version of this article.)

mean mass concentration of NO_3^- is observed in winter (12.7 ± 18.7 μg m^{-3}). The slightly lower mass concentration of NO_3^- in summer is related to both the lower level of NO_2 (Fig. 3d) and the gas-particle partitioning of NO_3^- in the warm season at high temperatures (Sciare et al., 2007). The seasonal cycle is similar to that observed in 2011–2012 in urban Beijing (Sun et al., 2015a, 2015b). The observed mean annual mass concentration of NO_3^- reported in that study was 18.0 ± 18.3 μg m^{-3} (reported as PM$_1$ and converted to PM$_{2.5}$ according to the ratio PM$_1$/PM$_{2.5} \approx 0.7$), indicating the decline in NO_3^- in recent years. The mean concentration of SO_4^{2-} (proportion of SO_4^{2-}) varies greatly in different seasons, ranging from 7.8 ± 16.0 μg m^{-3} (14%) in winter to 14.2 ± 10.2 μg m^{-3} (31%) in summer (Fig. 4a). The overall seasonal variations in mass concentration and fraction of SO_4^{2-} in this study are consistent with those observed in 2011–2012 in urban Beijing (Sun et al., 2015b) and in 2017–2018 (Zhou et al., 2019), when the highest mean mass concentrations of SO_4^{2-} were also observed in summer because of the strong photochemical formation and conversion of SO_2 to SO_4^{2-} (Zheng et al., 2011). For example, Y. L. Sun et al., 2015b observed that the mass concentrations of SO_4^{2-} were 11.0 ± 13.1 μg m^{-3} in winter and 15.1 ± 11.7 μg m^{-3} in summer. Note that the disparity in mass concentrations of SO_4^{2-} between winter and summer is larger in this

study due to the significantly decreased mass concentration of SO_4^{2-} in winter. This suggests that the reduction control measures conducted by the Chinese government mitigated SO_4^{2-} pollution in winter.

The ratio of NO_3^- to SO_4^{2-} varies seasonally (Fig. 4b). In winter, the mean concentration of NO_3^- was greater than that of SO_4^{2-} (with a mean ratio of 1.6 ± 1.2). This mean ratio is similar to what was observed in the winters of 2011–2015 in Beijing, i.e., ~1.5 (Fig. 5) (e.g. Dao et al., 2014; Sun et al., 2015b; Li et al., 2018; Li et al., 2019; Wu et al., 2020). However, the mean ratio is smaller than that observed in the winters of 2016–2017 in urban Beijing, with NO_3^- concentrations 2.5–3.5 times higher than SO_4^{2-} concentrations (Fig. 5) (Li et al., 2019). The ratio of NO_3^- to SO_4^{2-} increased continuously from about 0.5 in 1999–2000 (Yao et al., 2002) to as high as 3.5 in 2017 (Fig. 5) (Li et al., 2019), illustrating the increasingly dominant role of NO_3^-. This reflects a significant conversion of SO_4^{2-} to NO_3^- pollution in winter in China during the past 20 years, with the rapid reduction in SO_2 emissions but a continuous increase in NO_x emissions, especially from vehicle sources in urban areas (Zheng et al., 2018). Also, the direct reductions in primary SO_4^{2-} from coal burning sources in winter of Beijing (Dai et al., 2019) should also considerably contribute to the elevated ratio of NO_3^- to SO_4^{2-} during past years. The ratio of NO_3^- to SO_4^{2-} from this study is smaller than that observed in 2016–2017. This is partially associated with an attenuated nitrate formation likely due to reduced NO_x emissions since 2016 in China (Zheng et al., 2018; Xu et al., 2019). The decrease in SO_4^{2-} may also decrease aqueous production or gas-particle partitioning of NO_3^- due to the weakened hygroscopicity of aerosol particles (Li et al., 2019). The ratio of NO_3^- to SO_4^{2-} in winter is thus expected to decrease over the next few years, as NO_x emissions decline and SO_4^{2-} sources weakens.

In summer, SO_4^{2-} accounts for a larger proportion of SIA (31%, 14.2 μg m^{-3}) than NO_3^- (22%, 9.9 μg m^{-3}), yielding the smallest ratio of NO_3^- to SO_4^{2-} throughout the whole year. The mean ratio in this study is 0.7 ± 1.0, much lower than that observed in the summers of 2015–2017 (with ratios of ~2.0) (Li et al., 2018; Lv et al., 2019; Xu et al., 2019) and comparable to that observed before 2013 (Fig. 5). Note that the concentration of SO_4^{2-} in summer is still high even at very low SO_2 levels, which warrants further investigation in the future.

In summary, our results show that there was a turning point of decline in the ratio of NO_3^- to SO_4^{2-} in China in 2018–2019, before which the ratio had been increasing continuously since 1999. The average mass concentration of NO_3^- during 2018–2019 has been reduced compared with that observed during 2011–2012 (Sun et al., 2015a, 2015b). This is likely due to the decline in NO_x emissions since 2016 (Zheng et al., 2018). Our results suggest that the strict reduction control measures are efficient in improving SO_4^{2-} pollution in winter but not in summer. However, the two SIA, SO_4^{2-} and NO_3^- concentrations together still comprise 37–53% of the PM$_{2.5}$ concentration, presenting significant role in dominating the levels of PM$_{2.5}$.

3.3. Diurnal variations

Fig. 6 shows the diurnal cycles of mass concentrations of NO_3^- and SO_4^{2-}, mass fractions of NR-PM$_{2.5}$ chemical species, and the ratio NO_3^-/SO_4^{2-} for each season. In summer and autumn, the diurnal variations of NO_3^- are with minimum mass concentrations during the day (12:00–16:00 local time, or LT) and maximum mass concentrations at night (21:00–06:00 LT) (Fig. 6b and c). Three factors may explain this: (1) In warm seasons, due to the high ambient daytime temperature, gas-particle partitioning of NO_3^- causes the conversion of NO_3^- in the particle phase to the gas phase (Takahama, 2004), and thus decreasing the NO_3^- levels in daytime; (2) A large amount of NO_3^- is formed through the heterogeneous hydrolysis of N_2O_5 in the absence of ultraviolet light at night (Mentel et al., 1996), and thereby elevating its levels during nighttime, and (3) PBL heights are generally higher in the daytime than at night (Liu and Liang, 2010), which would further accumulate the NO_3^- concentrations. In winter, the mass concentration of NO_3^- continuously increases from 08:00 LT to 16:00 LT, probably due to the formation of
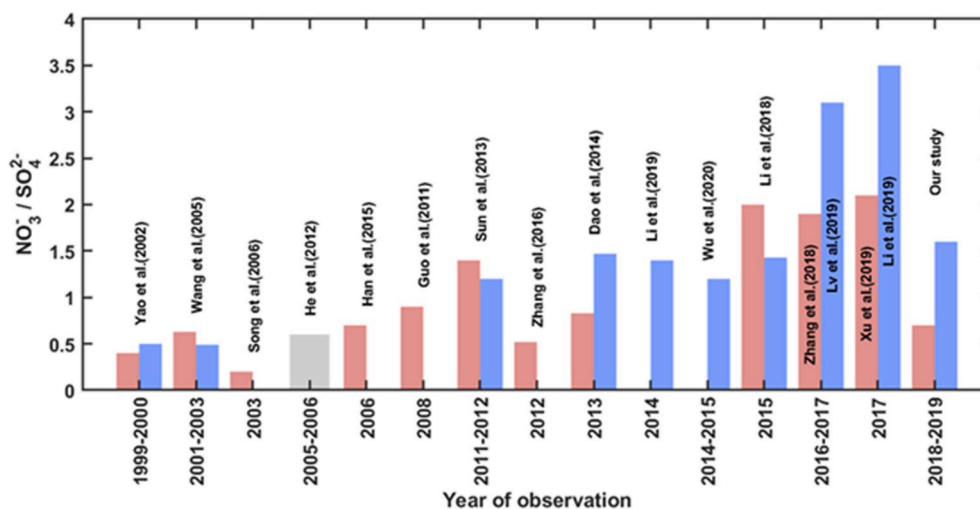
Fig. 5. The ratio NO_3^-/SO_4^{2-} from different studies, starting in 1999–2000 and ending in 2018–2019 (this study). Red bar represents summer, blue bar represents winter and gray bar represents the annual mean. (For interpretation of the references to color in this figure legend, the reader is referred to the Web version of this article) (Guo et al., 2011; Han et al., 2015; He et al., 2012; Liu et al., 2020; Song et al., 2006; Wang et al., 2005; Zhang et al., 2016).
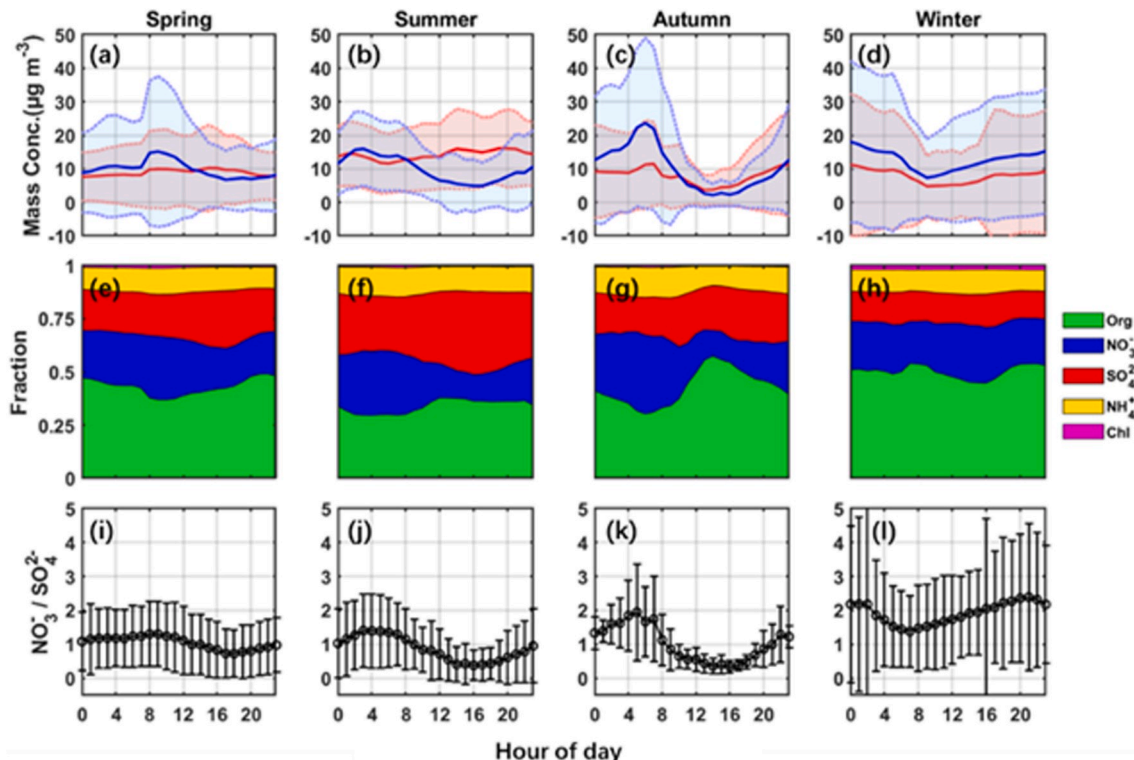

Fig. 6. Seasonal average diurnal cycles of **(a–d)** mass concentrations of sulfate (SO_4^{2-}, red) and nitrate (NO_3^-, blue), **(e–h)** mass fractions of NR-PM$_{2.5}$ chemical species, and **(i–l)** the ratio NO_3^-/SO_4^{2-}. (For interpretation of the references to color in this figure legend, the reader is referred to the Web version of this article.)

NO_3^- through the weak photochemical oxidation of NO_2 by the OH radical at sunrise when ambient temperatures are low (Ma et al., 2019). Overall, the mass concentration of NO_3^- is low in the daytime and high at night. This suggests the dominant role of the PBL in controlling the diurnal patterns of NO_3^- in cold seasons when photochemical processes are weaker.

In spring, the mass concentration of NO_3^- peaks between 08:00 LT and 12:00 LT. This is likely related to the nocturnal boundary layer (NBL) effect (Geyer, 2004). At night, there is a continuous emission of NO_x near the ground, which is not conducive to the production of N_2O_5. However, high concentrations of NO_2 still exist in the upper NBL, which

has temperature conditions more conducive to the accumulation of N_2O_5. Therefore, in the upper NBL at night, a large amount of NO_3^- will be generated through the hydrolysis of N_2O_5. Until the sun rises, the vertical turbulence caused by the changes in ambient temperature will transport the NO_3^- already formed at high altitudes within the NBL, resulting in a sudden rise in the concentration of NO_3^- on the ground in the morning. This may explain why the peak in the morning is only observed in spring. However, this still needs further verification.

The amplitudes of the diurnal cycles of SO_4^{2-} are much smaller than those of NO_3^-, varying little from season to season. This is because the formation of SO_4^{2-} from photochemical oxidation by SO_2 is very slow
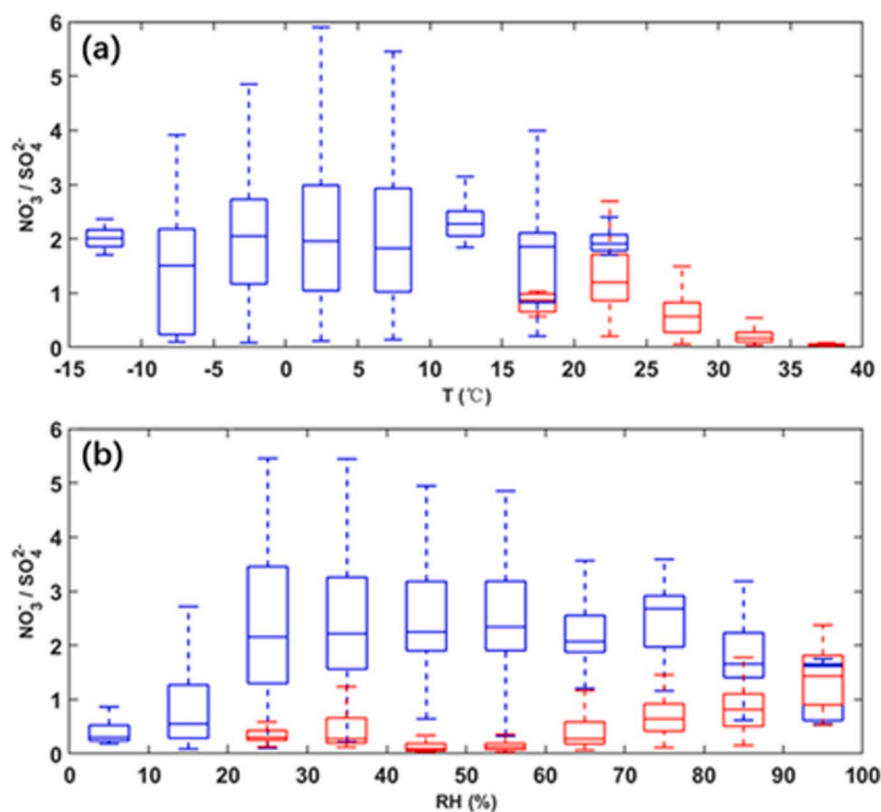
Fig. 7. Variations in the ratio NO_3^-/SO_4^{2-} as a function of **(a)** T and **(b)** RH in cold seasons (blue boxes) and warm seasons (red boxes). Horizontal lines in the box plot represent the median values, upper and lower borders of the box represent the 25th and 75th percentile values, and the upper and lower borders of the dashed vertical lines represent the 10th and 90th percentile values. (For interpretation of the references to color in this figure legend, the reader is referred to the Web version of this article.)

with a time scale of one week (Cox, 1979). The slight fluctuations are mainly influenced by variations in the PBL and meteorology. Fig. 6i-l shows the diurnal cycles of the ratio NO_3^-/SO_4^{2-} in different seasons. Since the diurnal cycles of SO_4^{2-} vary little from season to season, the diurnal cycles of NO_3^-/SO_4^{2-} show similar patterns to the diurnal variations of mass concentration of NO_3^- in all seasons.

3.4. Impacts of T and RH on the ratio of NO_3^- to SO_4^{2-}

The mass ratio of NO_3^- to SO_4^{2-} generally varies under different meteorological conditions (humidity and RH) and is an indicator of local and transmitted sources of pollution (Arimoto et al., 1996; Yao et al., 2002). To obtain insights of the effect of the temperature and RH on the nitrate and sulfate formation, in this study, we analyzed the dependence of the ratio of NO_3^- to SO_4^{2-} on temperature and relative humidity (RH) in cold seasons (winter and spring) and warm seasons (summer and autumn) (Fig. 7).

The ratio NO_3^-/SO_4^{2-} in cold seasons varies little as T increases from −15 °C to 20 °C. The ratio decreases from ∼2.0 in winter to nearly 0 as T increases from 20 °C to 40 °C in warm seasons. The sensitivity of the ratio to changes in T reflects the enhanced gas-particle partitioning of NO_3^- to the gaseous state at high temperatures (Takahama, 2004). Here, the threshold value for NO_3^- partitioning is 20 °C, consistent with that previously reported by (Li et al., 2018).

The dependence of the ratio NO_3^-/SO_4^{2-} on RH is more pronounced. In cold seasons, NO_3^-/SO_4^{2-} increases from about 0.5 to greater than 2 with increasing RH under very dry atmospheric conditions in Beijing (RH < 40%). The ratio remains constant (∼2.2) in the RH range of 20–80%, decreasing slightly when RH > 80%. The slight reduction at very high RH levels is likely associated with an enhanced aqueous formation or in-cloud SO_4^{2-} oxidation over urban Beijing in winter (Wang et al., 2016). The variations of the ratios with RH is also likely associated with the changes of PBL (see Section 3.5). In warm seasons, the ratio NO_3^-/SO_4^{2-} generally increase with increasing RH from about 0.1 to 1.

This is due to the enhanced NO_3^- formation through the heterogeneous hydrolysis of N_2O_5 at high RH levels during the night.

Others have examined the relationships between NO_3^-/SO_4^{2-} and T and RH. For example, Y. L. Sun et al., 2013b found that the ratio NO_3^-/SO_4^{2-} was positively correlated with RH in summer in urban Beijing from 2011 to 2012 and that the ratio fluctuated in the range of 0.5–2, consistent with findings from this study. They also found that the ratio decreased from 2.2 to 0.7 as RH increased from 10% to 90% in winter. Li et al. (2018) also observed that the mass ratio of NO_3^- to SO_4^{2-} increased from about 0.5 to ∼4 as temperatures decreased from 40 °C to 20 °C) and as RH increased from 20% to 90% in the summer of 2015 in Beijing. The ratios are much larger than in 2011–2012, which closer to our observations in winter.

3.5. Case studies: attributing the rapid increase in ambient NO_3^- under different meteorological conditions

To further elucidate the mechanism and formation of NO_3^- in fine particles in urban Beijing, two periods, representing typical cases of the rapid growth of the mass concentration of NO_3^- in a short time during the observation period (Fig. 8) are selected for analysis. Used were the ratios of SO_4^{2-} and NO_3^- to BC or carbon monoxide (CO) (due to the unavailability of BC data for Case 1) to eliminate the influence of the PBL on the variations in NO_3^- and SO_4^{2-} concentrations because the physical and chemical properties of CO and BC are relatively stable within the PBL (Zhang et al., 2015a,b). Fig. 9a shows a typical case (defined as Case 1) of a burst in the mass concentration of NO_3^- during a heavy haze event that occurred on 11–14 March 2018. The $PM_{2.5}$ concentration was 175.8 ± 73.8 μg m^{-3}, reaching a maximum value of ∼400 μg m^{-3} (Fig. 9). The winds show static meteorological conditions. The mean RH and T were 54.2% and 8.7 °C, respectively, and varied diurnally. The mean concentrations of O_3, SO_2, NO_2, and CO were 61.1, 14.1, 85.1, and 1720.0 μg m^{-3}, respectively. The mass concentration of NO_3^- increased rapidly from 11.9 μg m^{-3} to nearly 100.0 μg m^{-3} within 60 h. The mass
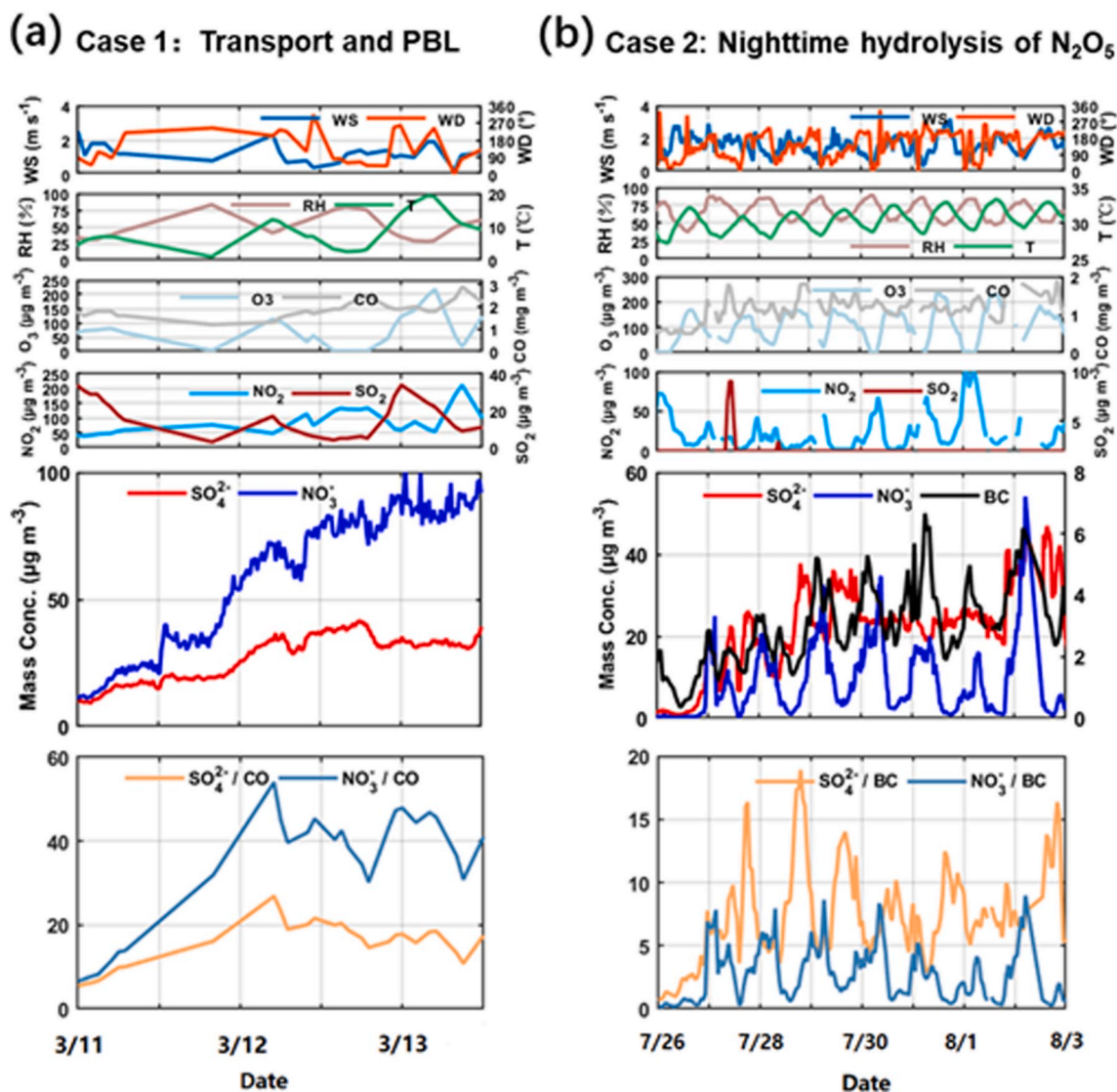
Fig. 8. Time series of meteorological parameters (wind speed,WS, wind direction, WD, relative humidity, RH, and temperature, T), gaseous precursors (O$_3$, CO, NO$_2$, and SO$_2$), mass concentrations of SO$_4^{2-}$, NO$_3^-$, and BC, and ratios of SO$_4^{2-}$and NO$_3^-$ to BC and CO for **(a)** Case 1 and **(b)** Case 2. Data are from 11 to 13 March 2018 (left panels) and 26 July to 3 August 2018 (right panels).

concentration of SO$_4^{2-}$ also rapidly grew from about 10 μg m^{-3} to 40.7 μg m^{-3}. However, the ratios SO$_4^{2-}$/CO and NO$_3^-$/CO showed continuous increases only before 14:00 LT on 12 March, then stabilized. Further investigation of the variations in the PBL retrieved from lidar data (Fig. 9) shows that the height of the PBL was ~1.0 km and remained that way before 12:00 LT on March 12, after which the height of the PBL decreased to 200–300 m. This suggests that the observed fast increase in mass concentrations of NO$_3^-$ and SO$_4^{2-}$ after 12:00 LT on March 12 was mainly due to the sharp decrease in the PBL height. The growth before 12:00 LT on March 12 was likely due to other sources, e.g., secondary formation or transport. Some studies have shown that NO$_3^-$ formation in springtime is facilitated by dust through heterogeneous processes (Xia et al., 2019). However, our data show that the mass concentrations of PM$_{10}$ were almost the same as those of PM$_{2.5}$, suggesting that coarse-mode aerosols were negligible (Fig. 9b). Note that winds were light (<2 m s^{-1}) and coming from the south or southwest. The continuous growth before 12:00 LT on March 12 is thus attributed to the regional transport of air pollution from populated regions south of urban Beijing.

Fig. 8b shows a typical case (defined as Case 2) of warm-season variations in NO$_3^-$ that occurred from 26 July to 3 August 2018 in

urban Beijing. During this case, the mean PM$_{2.5}$ concentration was 56.5 ± 26.9 μg m^{-3}. Winds were steady and light. RH and T varied diurnally, with mean values of 68.5% and 31.4 °C. The mean concentrations of O$_3$, SO$_2$, NO$_2$, and CO were 105.6, 2.1, 23.3, and 1200 μg m^{-3}, respectively. Both O$_3$ and NO$_2$ also varied diurnally, with SO$_2$ concentrations approaching the lower limit of detection (2 μg m^{-3}). NO$_3^-$ varied diurnally, with a maximum value at night and a minimum value during the day, indicating the heterogeneous hydrolysis formation from N$_2$O$_5$ at night and conversion of NO$_3^-$ in particle phase to the gas phase during the warmer daytime. It has been known that, nitrogen dioxide reacts with ozone to produce the NO$_3$ radical, and the latter further reacts with NO$_2$, forming N$_2$O$_5$. N$_2$O$_5$ is prone to photolysis or thermal deposition and is stable at night. In addition to the daytime gas-phase formation of HNO$_3$, the hydrolysis of N$_2$O$_5$ with aerosols and fog is a major source of nitric acid in the urban atmosphere at night (Pathak et al., 2009). This reaction proceeds efficiently on wet surfaces but slowly in the gas phase (Wahner et al., 1998). Fig. 10 further confirms this, showing good agreements between the ratio SO$_4^{2-}$/BC with RH and T (correlation co-efficients of 0.72 and −0.69, respectively). Also, the higher the RH, or the lower the T, the faster the growth rate of NO$_3^-$ is (here, the growth rate at a given time is the slopes of the NO$_3^-$ and observation time).
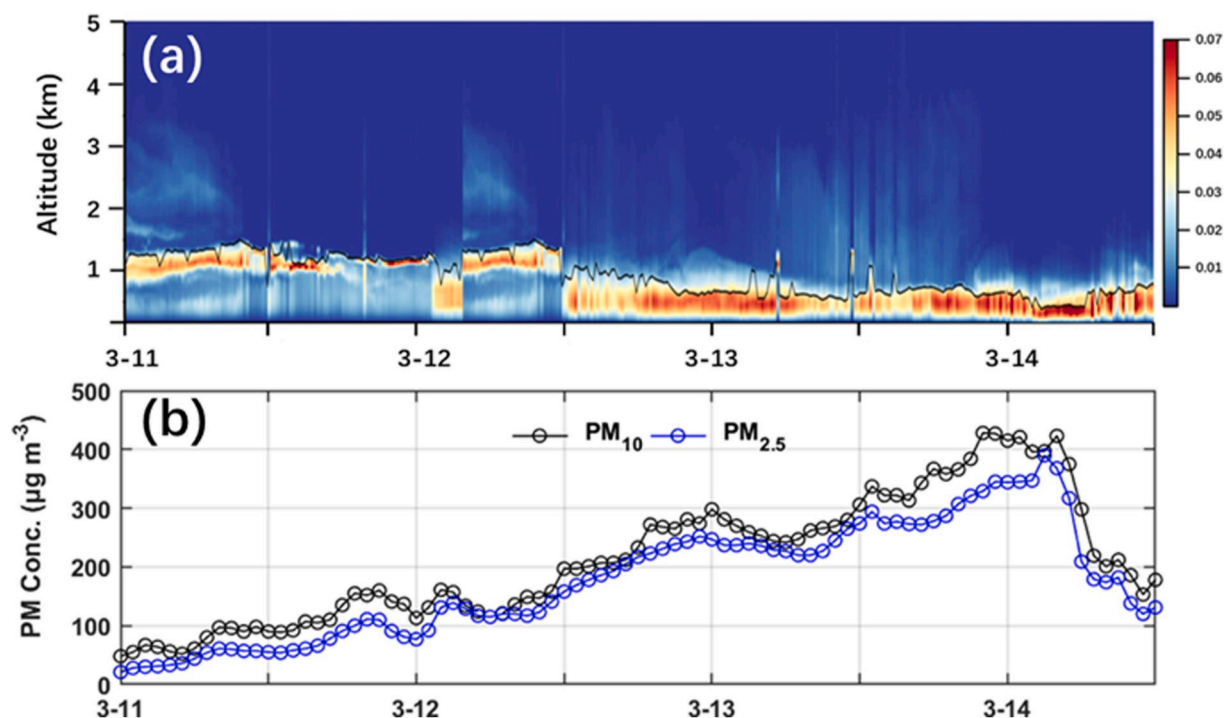
Fig. 9. Time series of **(a)** the planetary boundary layer height retrieved from lidar observations. The black line represents the top of the PBL, and the colors indicate the magnitudes of the extinction coefficients. **(b)** PM$_{2.5}$ (in blue) and PM$_{10}$ (in black) concentrations during the Case 1 haze formation process. (For interpretation of the references to color in this figure legend, the reader is referred to the Web version of this article.)

However, it shows different patterns for Case 2, implying distinct atmospheric processes of accumulation of nitrate for the two cases.

In summary, Case 1 and Case 2 represent two typical processes leading to the rapid accumulation and increase in NO_3^- in the atmosphere over urban Beijing. The mean background NO_3^- concentration during the cold-season Case 1 was 3.4 ± 3.5 μg m^{-3}, increasing to 51.2 ± 26.4 μg m^{-3} due to the regional transportation and PBL variations. The mean background NO_3^- concentration during the warm-season Case 2 was 2.0 ± 1.4 μg m^{-3}, increasing to 15.9 ± 9.5 μg m^{-3} due to the nighttime hydrolysis of N_2O_5. The Case 1 scenario contributes to heavy haze in cold seasons, while the Case 2 scenario impacts the diurnal patterns of NO_3^- in warm seasons.

4. Conclusions

In this study, the ratio of NO_3^- to SO_4^{2-} in fine particles is characterized using Q-ACSM -measured non-refractory submicron aerosol data in the urban area of Beijing from March 2018 to February 2019. We show that the ratio of NO_3^- to SO_4^{2-} varies seasonally, with a maximum value in winter (1.6 ± 1.2) and a minimum in summer (0.7 ± 1.0). Based on a literature review of results from earlier studies, the ratio of NO_3^- to SO_4^{2-} in China had been increasing continuously since 1999–2000 but started to decrease in 2018–2019. The mean concentration of NO_3^- was also lower compared with that in earlier years. We attribute the observed turning point (2018–2019) to the decrease in NO_x emissions since 2016 (Zheng et al., 2018). The ratio of NO_3^- to SO_4^{2-} in winter is expected to decrease over the next few years, as NO_x emissions decline and SO_4^{2-} sources (both primary emissions from coal burning and secondary formation) weakens. The mass concentration of SO_4^{2-} in summer is comparable to that observed in earlier years. Our results suggest that the strict reduction control measures in place serve only to improve SO_4^{2-} pollution in winter but not in summer. SO_4^{2-} and NO_3^- concentrations together comprise 37–53% of the PM$_{2.5}$ concentration, presenting key role in dominating the levels of PM$_{2.5}$.

Our results also show that the gas-particle partitioning of NO_3^- and

the hydrolysis of N_2O_5 regulate the diurnal cycle of the ratio NO_3^-/SO_4^{2-} in summer, while variations in the PBL height dominate it in winter. The dependence of the ratio NO_3^-/SO_4^{2-} on RH is more pronounced in cold seasons. In warm seasons, the ratio generally increases with increasing RH due to enhanced NO_3^- formation through the heterogeneous hydrolysis of N_2O_5 at high RH levels. We finally characterize two typical processes that lead to the rapid accumulation and increase in NO_3^- in the atmosphere over urban Beijing: (1) regional transportation and PBL variations and (2) the hydrolysis of N_2O_5. We find that the former contributes to heavy haze in cold seasons and that the latter tends to impact the diurnal variations in NO_3^- in warm seasons.

Data availability

All data needed to evaluate the conclusions in the paper are present in the paper. Also, all data used in the study are available from the corresponding author upon request (fang.zhang@bnu.edu.cn).

Author contributions

F.Z. and S.L. conceived the conceptual development of the manuscript. S. L. directed and performed of the experiments with L.C., X.J., H. W., J. L. and F. Z. S.L. and F.Z. conducted the data analysis and wrote the draft of the manuscript, and all authors edited and commented on the various sections of the manuscript.

Declaration of competing interest

The authors declare that they have no known competing financial interests or personal relationships that could have appeared to influence the work reported in this paper.

CRediT authorship contribution statement

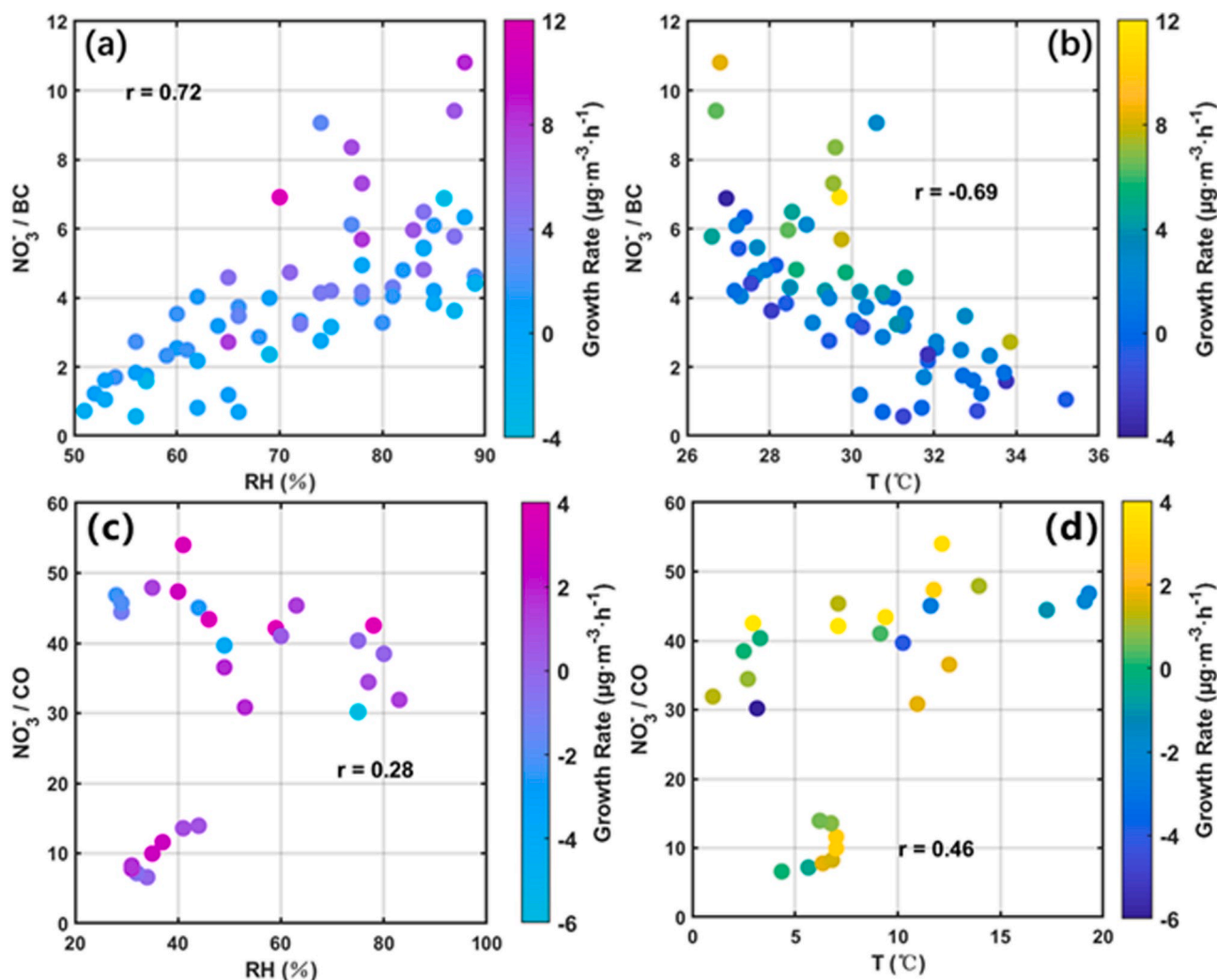**Shangze Li:** Writing - original draft, Formal analysis, Methodology.

Fig. 10. Dependence of the ratio NO_3^-/BC on **(a)** relative humidity (RH) and **(b)** temperature (T) for Case 2 and the ratio NO_3^-/CO on **(c)** relative humidity (RH) and **(d)** temperature (T) for Case 1. The color bar on the right represents the growth rate of NO_3^-. (For interpretation of the references to color in this figure legend, the reader is referred to the Web version of this article.)

Fang Zhang: Writing - original draft, Writing - review & editing, Conceptualization, Funding acquisition. **Xiaoai Jin:** Writing - review & editing. **Yele Sun:** Writing - review & editing. **Hao Wu:** Writing - review & editing. **Conghui Xie:** Writing - review & editing. **Lu Chen:** Writing - review & editing. **Jieyao Liu:** Writing - review & editing. **Tong Wu:** Writing - review & editing. **Sihui Jiang:** Writing - review & editing. **Maureen Cribb:** Writing - review & editing. **Zhanqing Li:** Writing - review & editing.

Acknowledgements

Appendix A. Supplementary data

Supplementary data to this article can be found online at https://doi.org/10.1016/j.atmosenv.2020.117662.

References

Allan, J.D., Jimenez, J.L., Williams, P.I., Alfarra, M.R., Bower, K.N., Jayne, J.T., Coe, H., Worsnop, D.R., 2003. Quantitative sampling using an Aerodyne aerosol mass spectrometer. 1. Techniques of data interpretation and error analysis. J. Geophys. Res. Atmos. 108 https://doi.org/10.1029/2002jd002358.

An, Z., Huang, R.J., Zhang, R., Tie, X., Li, G., Cao, J., Zhou, W., Shi, Z., Han, Y., Gu, Z., Ji, Y., 2019. Severe haze in northern China: a synergy of anthropogenic emissions and atmospheric processes. Proc. Natl. Acad. Sci. U.S.A. 116, 8657–8666. https://doi.org/10.1073/pnas.1900125116.

Arimoto, R., Duce, R.A., Savoie, D.L., Prospero, J.M., Talbot, R., Cullen, J.D., Tomza, U., Lewis, N.F., Ray, B.J., 1996. Relationships among aerosol constituents from asia and the north pacific during PEM-west A. J. Geophys. Res. Atmos. 101, 2011–2023. https://doi.org/10.1029/95jd01071.

Cox, R.A., 1979. Photochemical oxidation of atmospheric sulphur dioxide. Phil. Trans. Roy. Soc. Lond. Math. Phys. Sci. 290, 543–550. https://doi.org/10.1098/rsta.1979.0013,1979.

Dai, Q., Bi, X., Song, W., Li, T., Liu, B., Ding, J., Xu, J., Song, C., Yang, N., Schulze, B.C., Zhang, Y., Feng, Y., Hopke, P.K., 2019. Residential coal combustion as a source of primary sulfate in Xi'an, China. Atmos. Environ. 196, 66–76. https://doi.org/10.1016/j.atmosenv.2018.10.002.

Dao, X., Wang, Z., Lv, Y., Teng, E., Zhang, L., Wang, C., 2014. Chemical characteristics of water-soluble ions in particulate matter in three metropolitan areas in the North China Plain. PloS One 9, e113831. https://doi.org/10.1371/journal.pone.0113831.

Drewnick, F., Hings, S.S., DeCarlo, P., Jayne, J.T., Gonin, M., Fuhrer, K., Weimer, S., Jimenez, J.L., Demerjian, K.L., Borrmann, S., Worsnop, D.R., 2005. A new Time-of-Flight Aerosol Mass Spectrometer (TOF-AMS)—instrument description and first field deployment. Aerosol Sci. Technol. 39, 637–658. https://doi.org/10.1080/02786820500182040.

Geyer, A., 2004. Vertical profiles of NO_3, N_2O_5, O_3, and NO_x in the nocturnal boundary layer. 2. Model studies on the altitude dependence of composition and chemistry. J. Geophys. Res. Atmos 109 https://doi.org/10.1029/2003jd004211.

Guo, H., Sullivan, A.P., Campuzano-Jost, P., Schroder, J.C., Lopez-Hilfiker, F.D., Dibb, J. E., Jimenez, J.L., Thornton, J.A., Brown, S.S., Nenes, A., Weber, R.J., 2016. Fine particle pH and the partitioning of nitric acid during winter in the northeastern United States. J. Geophys. Res. Atmos. 121 (10) https://doi.org/10.1002/2016jd025311, 355–310,376.

Guo, S., Hu, M., Zamora, M.L., Peng, J., Shang, D., Zheng, J., Du, Z., Wu, Z., Shao, M., Zeng, L., Molina, M.J., Zhang, R., 2014. Elucidating severe urban haze formation in China. Proc. Natl. Acad. Sci. U.S.A. 111, 17373–17378. https://doi.org/10.1073/pnas.1419604111.

Guo, Z., Bao, X., Chen, T., Chen, T., Zhou, F., Dong, Q., Lin, M., 2011. Mass concentration characteristics and source apportionment of water-soluble inorganic ions in aerosol in Beijing during 2008 Beijing Olympic Games. Trans. Atmos. Sci. (in Chinese) 34, 683–687. https://doi.org/10.1016/B978-0-444-53599-3.10005-8.

Han, T., Liu, X., Zhang, Y., Qu, Y., Zeng, L., Hu, M., Zhu, T., 2015. Role of secondary aerosols in haze formation in summer in the Megacity Beijing. J. Environ. Sci. (China). 31, 51–60. https://doi.org/10.1016/j.jes.2014.08.026.

He, K., Zhao, Q., Ma, Y., Duan, F., Yang, F., Shi, Z., Chen, G., 2012. Spatial and seasonal variability of $PM_{2.5}$ acidity at two Chinese megacities: insights into the formation of secondary inorganic aerosols. Atmos. Chem. Phys. 12, 1377–1395. https://doi.org/10.5194/acp-12-1377-2012.

Hu, W., Campuzano-Jost, P., Day, D.A., Croteau, P., Canagaratna, M.R., Jayne, J.T., Worsnop, D.R., Jimenez, J.L., 2017. Evaluation of the new capture vapourizer for aerosol mass spectrometers (AMS) through laboratory studies of inorganic species. Atmos. Meas. Tech. 10, 2897–2921. https://doi.org/10.5194/amt-10-2897-201.

Hu, W., Day, D.A., Campuzano-Jost, P., Nault, B.A., Park, T., Lee, T., Croteau, P., Canagaratna, M.R., Jayne, J.T., Worsnop, D.R., Jimenez, J.L., 2018. Evaluation of the new capture vaporizer for aerosol mass spectrometers: characterization of organic aerosol mass spectra. Aerosol Sci. Technol. 52, 725–739. https://doi.org/10.1080/02786826.2018.1454584.

Intergovernmental Panel on Climate Change (IPCC): Climate Change 2013, 2013. The Physical Science Basis. Contribution of Working Group I to the Fifth Assessment Report of the Intergovernmental Panel on Climate Change. Cambridge University Press, Cambridge, UK and New York, NY, USA.

Itahashi, S., Yumimoto, K., Uno, I., Hayami, H., Fujita, S.-i., Pan, Y., Wang, Y., 2018. A 15-year record (2001–2015) of the ratio of nitrate to non-sea-salt sulfate in precipitation over East Asia. Atmos. Chem. Phys. 18, 2835–2852. https://doi.org/10.5194/acp-18-2835-2018.

Jayne, J.T., Leard, D.C., Zhang, X., Davidovits, P., Smith, K.A., Kolb, C.E., Worsnop, D.R., 2000. Development of an aerosol mass spectrometer for size and composition analysis of submicron particles. Aerosol. Sci. Technol. 33, 49–70. https://doi.org/10.1080/027868200410840.

Li, H., Zhang, Q., Zheng, B., Chen, C., Wu, N., Guo, H., Zhang, Y., Zheng, Y., Li, X., He, K., 2018. Nitrate-driven urban haze pollution during summertime over the North China Plain. Atmos. Chem. Phys. 18, 5293–5306. https://doi.org/10.5194/acp-18-5293-2018.

Li, H., Cheng, J., Zhang, Q., Zheng, B., Zhang, Y., Zheng, G., He, K., 2019. Rapid transition in winter aerosol composition in Beijing from 2014 to 2017: response to clean air actions. Atmos. Chem. Phys. 19 (11) https://doi.org/10.5194/acp-19-11485-2019, 485–11,499.

Liu, S., Liang, X.-Z., 2010. Observed diurnal cycle climatology of planetary boundary layer height. J. Clim. 23, 5790–5809. https://doi.org/10.1175/2010jcli3552.1.

Liu, T., Clegg, S.L., Abbatt, J.P.D., 2020. Fast oxidation of sulfur dioxide by hydrogen peroxide in deliquesced aerosol particles. Proc. Natl. Acad. Sci. U.S.A. 117, 1354–1359. https://doi.org/10.1073/pnas.1916401117.

Lv, D., Chen, Y., Zhu, T., Li, T., Shen, F., Li, X., Mehmood, T., 2019. The pollution characteristics of PM_{10} and $PM_{2.5}$ during summer and winter in Beijing, Suning and Islamabad. Atmos. Pollut. Res. 10, 1159–1164. https://doi.org/10.1016/j.apr.2019.01.021.

Ma, X., Tan, Z., Lu, K., Yang, X., Liu, Y., Li, S., Li, X., Chen, S., Novelli, A., Cho, C., Zeng, L., Wahner, A., Zhang, Y., 2019. Winter photochemistry in Beijing: observation and model simulation of OH and HO_2 radicals at an urban site. Sci. Total Environ. 685, 85–95. https://doi.org/10.1016/j.scitotenv.2019.05.329.

Mentel, T.H.F., Bleilebens, D., Wahner, A., 1996. A study of nighttime nitrogen oxide oxidation in a large reaction chamber - the fate of NO_2 N_2O_5, HNO_3, and O-3 at different humidities. Atmos. Environ. 30, 4007–4020. https://doi.org/10.1016/1352-2310(96)00117-3.

Morgan, W.T., Ouyang, B., Allan, J.D., Aruffo, E., Di Carlo, P., Kennedy, O.J., Lowe, D., Flynn, M.J., Rosenberg, P.D., Williams, P.I., Jones, R., McFiggans, G.B., Coe, H., 2015. Influence of aerosol chemical composition on N_2O_5 uptake: airborne regional measurements in northwestern Europe. Atmos. Chem. Phys. 15, 973–990. https://doi.org/10.5194/acp-15-973-2015.

Ng, N.L., Herndon, S.C., Trimborn, A., Canagaratna, M.R., Croteau, P.L., Onasch, T.B., Sueper, D., Worsnop, D.R., Zhang, Q., Sun, Y.L., Jayne, J.T., 2011. An Aerosol Chemical Speciation Monitor (ACSM) for routine monitoring of the composition and mass concentrations of ambient aerosol. Aerosol Sci. Technol. 45, 780–794. https://doi.org/10.1080/02786826.2011.560211.

Pathak, R.K., Wu, W.S., Wang, T., 2009. Summertime $PM_{2.5}$ ionic species in four major cities of China: nitrate formation in an ammonia-deficient atmosphere. Atmos. Chem. Phys. 9, 1711–1722. https://doi.org/10.5194/acp-9-1711-2009.

Sciare, J., Cachier, H., Sarda-Estève, R., Yu, T., Wang, X., 2007. Semi-volatile aerosols in Beijing (R.P. China): characterization and influence on various $PM_{2.5}$ measurements. J. Geophys. Res. Atmos. 112 https://doi.org/10.1029/2006jd007448.

Song, Y., Xu, D., Chai, Z., 2006. Determination and characterization of anionic species of PM10 and PM2.5 in China. Chin. J. Anal. Lab. 25, 80–85. https://doi.org/10.3969/j.issn.1000-0720.2006.02.024.

Sun, Y.L., Wang, Z., Dong, H., Yang, T., Li, J., Pan, X., Chen, P., Jayne, J.T., 2012. Characterization of summer organic and inorganic aerosols in Beijing, China with an aerosol chemical speciation monitor. Atmos. Environ. 51, 250–259. https://doi.org/10.1016/j.atmosenv.2012.01.013.

Sun, Y.L., Du, W., Wang, Q., Zhang, Q., Chen, C., Chen, Y., Chen, Z., Fu, P., Wang, Z., Gao, Z., Worsnop, D.R., 2015a. Real-time characterization of aerosol particle composition above the urban canopy in Beijing: insights into the interactions between the atmospheric boundary layer and aerosol chemistry. Environ. Sci. Technol. 49 (11) https://doi.org/10.1021/acs.est.5b02373, 340–11,347.

Sun, Y.L., Wang, Z.F., Du, W., Zhang, Q., Wang, Q.Q., Fu, P.Q., Pan, X.L., Li, J., Jayne, J., Worsnop, D.R., 2015b. Long-term real-time measurements of aerosol particle composition in Beijing, China: seasonal variations, meteorological effects, and source analysis. Atmos. Chem. Phys. 15 (10) https://doi.org/10.5194/acp-15-10149-2015, 149–10,165.

Sun, Y.L., Wang, Z., Fu, P., Jiang, Q., Yang, T., Li, J., Ge, X., 2013a. The impact of relative humidity on aerosol composition and evolution processes during wintertime in Beijing, China. Atmos. Environ. 77, 927–934. https://doi.org/10.1016/j.atmosenv.2013.06.019.

Sun, Y.L., Wang, Z.F., Fu, P.Q., Yang, T., Jiang, Q., Dong, H.B., Li, J., Jia, J.J., 2013b. Aerosol composition, sources and processes during wintertime in Beijing, China. Atmos. Chem. Phys. 13, 4577–4592. https://doi.org/10.5194/acp-13-4577-2013.

Takahama, S., 2004. Modeling the diurnal variation of nitrate during the pittsburgh air quality study. J. Geophys. Res. Atmos. 109 https://doi.org/10.1029/2003jd004149.

Tang, M.J., Thieser, J., Schuster, G., Crowley, J.N., 2012. Kinetics and mechanism of the heterogeneous reaction of N_2O_5 with mineral dust particles. Phys. Chem. Chem. Phys. 14, 8551–8561. https://doi.org/10.1039/c2cp40805h.

Vasilakos, P., Russell, A., Weber, R., Nenes, A., 2018. Understanding nitrate formation in a world with less sulfate. Atmos. Chem. Phys. 18 (12) https://doi.org/10.5194/acp-18-12765-2018, 765–12,775.

Wahner, A., Mentel, T.F., Sohn, M., 1998. Gas-phase reaction of N_2O_5 with water vapor: importance of heterogeneous hydrolysis of N_2O_5 and surface desorption of HNO_3 in a large Teflon chamber. Geophys. Res. Lett. 25, 2169–2172. https://doi.org/10.1029/98GL51596.

Wang, G., Zhang, R., Gomez, M.E., Yang, L., Levy Zamora, M., Hu, M., Lin, Y., Peng, J., Guo, S., Meng, J., Li, J., Cheng, C., Hu, T., Ren, Y., Wang, Y., Gao, J., Cao, J., An, Z., Zhou, W., Li, G., Wang, J., Tian, P., Marrero-Ortiz, W., Secrest, J., Du, Z., Zheng, J., Shang, D., Zeng, L., Shao, M., Wang, W., Huang, Y., Wang, Y., Zhu, Y., Li, Y., Hu, J., Pan, B., Cai, L., Cheng, Y., Ji, Y., Zhang, F., Rosenfeld, D., Liss, P.S., Duce, R.A., Kolb, C.E., Molina, M.J., 2016. Persistent sulfate formation from London fog to Chinese haze. Proc. Natl. Acad. Sci. U.S.A. 113 (13) https://doi.org/10.1073/pnas.1616540113, 630–13,635.

Wang, H., Xue, M., Zhang, X.Y., Liu, H.L., Zhou, C.H., Tan, S.C., Che, H.Z., Chen, B., Li, T., 2015. Mesoscale modeling study of the interactions between aerosols and PBL meteorology during a haze episode in Jing–Jin–Ji (China) and its nearby surrounding region. Part 1: aerosol distributions and meteorological features. Atmos. Chem. Phys. 15, 3257–3275. https://doi.org/10.5194/acp-15-3257-2015.

Wang, H., Lu, K., Chen, X., Zhu, Q., Wu, Z., Wu, Y., Sun, K., 2018. Fast particulate nitrate formation via N_2O_5 uptake aloft in winter in Beijing. Atmos. Chem. Phys. 18 (10) https://doi.org/10.5194/acp-18-10483-2018, 483–10,495.

Wang, S., Yin, S., Zhang, R., Yang, L., Zhao, Q., Zhang, L., Yan, Q., Jiang, N., Tang, X., 2019a. Insight into the formation of secondary inorganic aerosol based on high-time-resolution data during haze episodes and snowfall periods in Zhengzhou, China. Sci. Total Environ. 660, 47–56. https://doi.org/10.1016/j.scitotenv.2018.12.465.

Wang, Y., Chen, J., Wang, Q., Qin, Q., Ye, J., Han, Y., Li, L., Zhen, W., Zhi, Q., Zhang, Y., Cao, J., 2019b. Increased secondary aerosol contribution and possible processing on polluted winter days in China. Environ. Int. 127, 78–84. https://doi.org/10.1016/j.envint.2019.03.021.

Wang, Y., Zhuang, G., Tang, A., Yuan, H., Sun, Y., Chen, S., Zheng, A., 2005. The ion chemistry and the source of $PM_{2.5}$ aerosol in Beijing. Atmos. Environ. 39, 3771–3784. https://doi.org/10.1016/j.atmosenv.2005.03.013.

Wang, Z., Wang, W., Tham, Y.J., Li, Q., Wang, H., Wen, L., Wang, X., Wang, T., 2017. Fast heterogeneous N_2O_5 uptake and $ClNO_2$ production in power plant and industrial plumes observed in the nocturnal residual layer over the North China Plain. Atmos. Chem. Phys. 17 (12) https://doi.org/10.5194/acp-17-12361-2017, 361–12,378.

WHO, World Health Organization, 2018. Air Pollution. WHO. https://www.who.int/airpollution/en/.

Wu, X., Chen, B., Wen, T., Habib, A., Shi, G., 2020. Concentrations and chemical compositions of PM_{10} during hazy and non-hazy days in Beijing. J. Environ. Sci. (China) 87, 1–9. https://doi.org/10.1016/j.jes.2019.03.021.

Xia, M., Wang, W., Wang, Z., Gao, J., Li, H., Liang, Y., Yu, C., Zhang, Y., Wang, P., Zhang, Y., Bi, F., Cheng, X., Wang, T., 2019. Heterogeneous uptake of N_2O_5 in sand dust and urban aerosols observed during the dry season in Beijing. Atmosphere 10. https://doi.org/10.3390/atmos10040204.

Xu, P., Zhang, J., Ji, D., Liu, Z., Tang, G., Jiang, C., Wang, Y., 2018. Characterization of submicron particles during autumn in Beijing, China. J. Environ. Sci (China) 63, 16–27. https://doi.org/10.1016/j.jes.2017.03.036.

Xu, W.Q., Sun, Y., Wang, Q., Zhao, J., Wang, J., Ge, X., Xie, C., Zhou, W., Du, W., Li, J., Fu, P., Wang, Z., Worsnop, D.R., Coe, H., 2019b. Changes in aerosol chemistry from 2014 to 2016 in winter in Beijing: insights from high-resolution aerosol mass spectrometry. J. Geophys. Res. Atmos. 124, 1132–1147. https://doi.org/10.1029/2018jd029245.

Xu, Q., Wang, S., Jiang, J., Bhattarai, N., Li, X., Chang, X., Qiu, X., Zheng, M., Hua, Y., Hao, J., 2019a. Nitrate dominates the chemical composition of $PM_{2.5}$ during haze

event in Beijing, China. Sci. Total Environ. 689, 1293–1303. https://doi.org/10.1016/j.scitotenv.2019.06.294.

Xu, W., Croteau, P., Williams, L., Canagaratna, M., Onasch, T., Cross, E., Zhang, X., Robinson, W., Worsnop, D., Jayne, J., 2016. Laboratory characterization of an aerosol chemical speciation monitor with PM$_{2.5}$ measurement capability. Aerosol Sci. Technol. 51, 69–83. https://doi.org/10.1080/02786826.2016.1241859.

Xu, W., Sun, Y.L., Chen, C., Du, W., Han, T.T., Wang, Q.Q., Fu, P.Q., Wang, Z.F., Zhao, X.J., Zhou, L.B., Ji, D.S., Wang, P.C., Worsnop, D.R., 2015. Aerosol composition, oxidation properties, and sources in Beijing: results from the 2014 Asia-Pacific Economic Cooperation summit study. Atmos. Chem. Phys. 15 (13) https://doi.org/10.5194/acp-15-13681-2015, 681–13,698.

Yang, F., Tan, J., Zhao, Q., Du, Z., He, K., Ma, Y., Duan, F., Chen, G., Zhao, Q., 2011. Characteristics of PM$_{2.5}$ speciation in representative megacities and across China. Atmos. Chem. Phys. 11, 5207–5219. https://doi.org/10.5194/acp-11-5207-2011.

Yao, X., Chak, K., Fang, M., Steven, C., Chan, T., Patricia, M., He, K., Ye, B., 2002. The water-soluble ionic composition of PM$_{2.5}$ in Shanghai and Beijing, China. Atmos. Environ. Times 36, 4223–4234. https://doi.org/10.1016/S1352-2310(02)00342-4.

Yun, H., Wang, W., Wang, T., Xia, M., Yu, C., Wang, Z., Poon, S.C.N., Yue, D., Zhou, Y., 2018. Nitrate formation from heterogeneous uptake of dinitrogen pentoxide during a severe winter haze in southern China. Atmos. Chem. Phys. 18 (17) https://doi.org/10.5194/acp-18-17515-2018, 515–17,527.

Zhang, F., Wang, Y., Peng, J., Chen, L., Sun, Y., Duan, L., Ge, X., Li, Y., Zhao, J., Liu, C., Zhang, X., Zhang, G., Pan, Y., Wang, Y., Zhang, A.L., Ji, Y., Wang, G., Hu, M., Molina, M.J., Zhang, R., 2020. An unexpected catalyst dominates formation and radiative forcing of regional haze. Proc. Natl. Acad. Sci. U.S.A. https://doi.org/10.1073/pnas.1919343117.

Zhang, Y., Tang, L., Croteau, P.L., Favez, O., Sun, Y., Canagaratna, M.R., Wang, Z., Couvidat, F., Albinet, A., Zhang, H., Sciare, J., Prévôt, A.S.H., Jayne, J.T., Worsnop, D.R., 2017. Field characterization of the PM$_{2.5}$ Aerosol Chemical Speciation Monitor: insights into the composition, sources, and processes of fine particles in eastern China. Atmos. Chem. Phys. 17, 14501–14517. https://doi.org/10.5194/acp-17-14501-2017.

Zhang, R., Wang, G., Guo, S., Zamora, M.L., Ying, Q., Lin, Y., Wang, W., Hu, M., Wang, Y., 2015a. Formation of urban fine particulate matter. Chem. Rev. 115, 3803–3855. https://doi.org/10.1021/acs.chemrev.5b00067.

Zhang, Q., Quan, J., Tie, X., Li, X., Liu, Q., Gao, Y., Zhao, D., 2015b. Effects of meteorology and secondary particle formation on visibility during heavy haze events in Beijing, China. Sci. Total Environ. 502, 578–584. https://doi.org/10.1016/j.scitotenv.2014.09.079.

Zhang, Q., Ma, Q., Zhao, B., Liu, X., Wang, Y., Jia, B., Zhang, X., 2018. Winter haze over North China Plain from 2009 to 2016: influence of emission and meteorology. Environ. Pollut. 242, 1308–1318. https://doi.org/10.1016/j.envpol.2018.08.019.

Zhang, Q., Zheng, Y., Tong, D., Shao, M., Wang, S., Zhang, Y., Xu, X., Wang, J., He, H., Liu, W., Ding, Y., Lei, Y., Li, J., Wang, Z., Zhang, X., Wang, Y., Cheng, J., Liu, Y.,

Shi, Q., Yan, L., Geng, G., Hong, C., Li, M., Liu, F., Zheng, B., Cao, J., Ding, A., Gao, J., Fu, Q., Huo, J., Liu, B., Liu, Z., Yang, F., He, K., Hao, J., 2019. Drivers of improved PM$_{2.5}$ air quality in China from 2013 to 2017. Proc. Natl. Acad. Sci. U.S.A. 116 (24) https://doi.org/10.1073/pnas.1907956116, 463–24,469.

Zhang, Y., Huang, W., Cai, T., Fang, D., Wang, Y., Song, J., Hu, M., Zhang, Y., 2016. Concentrations and chemical compositions of fine particles (PM$_{2.5}$) during haze and non-haze days in Beijing. Atmos. Res. 174–175, 62–69. https://doi.org/10.1016/j.atmosres.2016.02.003.

Zheng, B., Tong, D., Li, M., Liu, F., Hong, C., Geng, G., Li, H., Li, X., Peng, L., Qi, J., Yan, L., Zhang, Y., Zhao, H., Zheng, Y., He, K., Zhang, Q., 2018. Trends in China's anthropogenic emissions since 2010 as the consequence of clean air actions. Atmos. Chem. Phys. 18 (14) https://doi.org/10.5194/acp-18-14095-2018, 095–14,111.

Zheng, J., Hu, M., Zhang, R., Yue, D., Wang, Z., Guo, S., Li, X., Bohn, B., Shao, M., He, L., Huang, X., Wiedensohler, A., Zhu, T., 2011. Measurements of gaseous H$_2$SO$_4$ by AP-ID-CIMS during CAREBeijing 2008 campaign. Atmos. Chem. Phys. 11, 7755–7765. https://doi.org/10.5194/acp-11-7755-2011.

Zhong, J., Zhang, X., Dong, Y., Wang, Y., Liu, C., Wang, J., Zhang, Y., Che, H., 2018. Feedback effects of boundary-layer meteorological factors on cumulative explosive growth of PM$_{2.5}$ during winter heavy pollution episodes in Beijing from 2013 to 2016. Atmos. Chem. Phys. 18, 247–258. https://doi.org/10.5194/acp-18-247-2018.

Zhou, W., Gao, M., He, Y., Wang, Q., Xie, C., Xu, W., Zhao, J., Du, W., Qiu, Y., Lei, L., Fu, P., Wang, Z., Worsnop, D.R., Zhang, Q., Sun, Y., 2019. Response of aerosol chemistry to clean air action in Beijing, China: insights from two-year ACSM measurements and model simulations. Environ. Pollut. 255, 113345. https://doi.org/10.1016/j.envpol.2019.113345.

Further reading

Fountoukis, C., Nenes, A., 2007. ISORROPIA II: a computationally efficient thermodynamic equilibrium model for K$^+$–Ca^{2+}–Mg^{2+}–NH^{+4}–Na$^+$–SO^{42-}–NO^{3-}–Cl$^-$–H^{2}O aerosols. Atmos. Chem. Phys. 7, 4639–4659. https://doi.org/10.5194/acp-7-4639-2007.

Song, S., Gao, M., Xu, W., Shao, J., Shi, G., Wang, S., Wang, Y., Sun, Y., McElroy, M.B., 2018. Fine-particle pH for Beijing winter haze as inferred from different thermodynamic equilibrium models. Atmos. Chem. Phys. 18, 7423–7438. https://doi.org/10.5194/acp-18-7423-2018.

Sun, Z., Mu, Y., Liu, Y., Shao, L., 2013c. A comparison study on airborne particles during haze days and non-haze days in Beijing. Sci. Total Environ. 456–457. https://doi.org/10.1016/j.scitotenv.2013.03.006, 1–8.

Wang, Y., Zhang, Q., Jiang, J., Zhou, W., Wang, B., He, K., Duan, F., Zhang, Q., Philip, S., Xie, Y., 2014. Enhanced sulfate formation during China's severe winter haze episode in January 2013 missing from current models. J. Geophys. Res. Atmos. 119 (10) https://doi.org/10.1002/2013jd021426, 425-410,440.